Conference on Modelling Fluid Flow (CMFF'22)
The 18th International Conference on Fluid Flow Technologies
Budapest, Hungary, August 30-September 2, 2022

COMPARISON OF OPENFOAM TURBULENCE MODELS FOR NUMERICAL SIMULATION OF THERMALLY-DRIVEN WINDS

Jose I. ROJAS[1], Santiago ARIAS[2], Rathan B. ATHOTA[2], Adeline MONTLAUR[2]

[1] Corresponding Author. Dept. of Physics - Division of Aerospace Eng., Universitat Politècnica de Catalunya. c/ Esteve Terradas 7, 08860, Castelldefels, Spain. Tel.: +34 93 413 4130, Fax: +34 93 413 7007, E-mail: josep.ignasi.rojas@upc.edu
[2] Dept. of Physics - Division of Aerospace Eng., Universitat Politècnica de Catalunya. E-mails: santiago.arias@upc.edu, rathan.babu.athota@upc.edu, adeline.de.montlaur@upc.edu

ABSTRACT

Commercial computational fluid dynamics (CFD) codes have often been used for simulation of atmospheric boundary layer (ABL) flows. The present work explores the potential of the open-source CFD software OpenFOAM for simulating thermally-driven winds, by comparing several turbulence models. Indeed, in ABL and other large-scale flows, turbulence is critical to the mixing process of momentum and buoyancy, and simulations with commercial CFD codes have usually been done with Reynolds-Averaged Navier-Stokes (RANS) turbulence modelling.

In this work, the formation of thermally-driven winds is studied in an idealised mountain-valley system, with realistic values of parameters such as the slope angle, the diurnal temperature cycle, etc. Performances of various OpenFOAM RANS turbulence models (k–ε, re-normalisation group (RNG) k–ε, k–ω shear stress transport (SST)) are compared. A preliminary study of LES using Smagorinsky closure is also contemplated. Velocity contours, velocity and temperature profiles, the shapes of vortexes/convective cells, and the computational times are presented for all the studied turbulence models, to help identify the most suitable one for simulation of thermally-driven winds.

Keywords: computational fluid dynamics (CFD), OpenFOAM, slope winds, thermally-driven winds, turbulence models

NOMENCLATURE

C_k	[−]	Kolmogorov constant
C_μ	[−]	turbulence viscosity ct.
D	[s^{-1}]	strain rate tensor
H_{ref}	[m]	reference height
N	[s^{-1}]	Brunt-Väisälä frequency
Pr	[−]	Prandtl number
T	[K]	temperature
T_E	[s]	Earth diurnal period
U_{ref}	[ms^{-1}]	reference velocity
W	[m]	valley width
c_p	[$Jkg^{-1}K^{-1}$]	specific heat at ct. pressure
h	[$Wm^{-2}K^{-1}$]	convective heat transfer coef.
k	[m^2s^{-2}]	turbulence kinetic energy
p	[Pa]	static pressure
p_{rgh}	[Pa]	dynamic pressure
p_T	[Pa]	total pressure
q_k	[Kms^{-1}]	kinematic heat flux
t	[s]	time
u^*	[ms^{-1}]	friction velocity
z_0	[m]	roughness length scale
U	[ms^{-1}]	flow velocity
$\vec{g}$	[ms^{-2}]	gravity acceleration vector
$\vec{r}$	[ms^{-1}]	position vector
α	[°]	slope angle
α_{ef}	[m^2s^{-1}]	effective thermal diffusivity
β	[K^{-1}]	volumen expansion coef.
κ	[−]	Von Kármán ct.
μ	[$kgm^{-1}s^{-1}$]	dynamic viscosity
ν	[m^2s^{-1}]	molecular kinematic viscosity
ν_{ef}	[m^2s^{-1}]	effective kinematic viscosity
ω	[s^{-1}]	turb. specific dissipation rate
ρ	[kgm^{-3}]	density
θ_*	[K]	potential temperature
ε	[m^2s^{-3}]	turbulence dissipation rate

Subscripts and Superscripts

0	sea level
x, z	along-slope, slope-normal coordinates
max	maximum
t	turbulent
X, Y, Z	width, depth and height coordinates
∞	free stream or far field

1. INTRODUCTION

Commercial computational fluid dynamics (CFD) codes have frequently been used for simulating atmospheric boundary layer (ABL) flows,

e.g., for wind energy applications. However, to increase the ability to create individualised solutions, and in a context of sometimes limited scientific funding, availability of open-source CFD software such as OpenFOAM is very attractive, especially as it has proven to be very useful for simulating ABL flows [1]. This is why, in this work, the potential of OpenFOAM for simulating a type of ABL flows (*i.e.*, thermally-driven winds) is explored, by studying several OpenFOAM turbulence models for simulating such flows. Indeed, in ABL and other large-scale flows, turbulence is critical to the mixing process of momentum and buoyancy [2]. In this regard, simulations of ABL flows with commercial CFD codes have been usually done with Reynolds-Averaged Navier-Stokes (RANS) turbulence modelling, applying the standard k–ε model [1, 3], the realisable k–ε model [4], or other modified k–ε models [1, 5]. The standard k–ε model has also been used in similar studies conducted with OpenFOAM [6].

Other possible RANS turbulence models are the k–ω shear stress transport (SST) model and the k–kl–ω turbulence model [7, 8, 9, 10, 11]. The latter is an extension of the k–ω SST model that includes laminar-turbulent transition prediction [12]. Numerical simulations have also been done considering the solution of the RANS, LES model, and 2-layer turbulence model [13], or have incorporated LES in the calculation, using a DES approach to solve the flow near walls (DES incorporates buoyancy, stratification, developed turbulence and complex topography) [14]. DES is a suitable option for making the most of the advantages of LES for modelling turbulent ABL flows, without the high computational cost associated with using LES in complex geometries or topographies [15]. Similarly, Favre-averaged Navier-Stokes eqs. have also been used to predict turbulent flows. To close this system of eqs., transport eqs. are used for turbulence kinetic energy (TKE) and its dissipation rate [16]. Finally, implementing non-linear k–ε turbulence models is also under consideration, as this could lead to better performance of the numerical model [1], particularly for prediction of TKE.

As per, OpenFOAM standard k–ε model RANS turbulence was used to simulate the wind flow over Mount Saint Helens, USA [17], over the Giza Plateau in Egypt [18], and convective winds in the Aburra open valley, Medellín, Colombia [19]. OpenFOAM was also used to study non-buoyant wind flows over complex terrains using RANS turbulence models with wall functions, to make accurate predictions of wind power production [20]. Finally, an OpenFOAM solver was developed using LES to simulate buoyant flows within the Boussinesq approach, focusing on flow interaction with wind turbines [21].

In this work, the diurnal cycle for thermally-driven winds is studied in an idealised mountain-valley system with realistic values of several parameters such as the slope angle, diurnal temperature profile, etc. The performance of various OpenFOAM RANS turbulence models (k–ε, re-normalisation group (RNG) k–ε, k–ω SST [7, 8, 9, 10, 11]) is compared. A preliminary study of LES with Smagorinsky closure [22, 23] is also presented on the same mesh used as for RANS simulations.

2. METHODOLOGY

The numerical method used in this work (including the governing eqs. based on the Boussinesq approach, main hypotheses, solver, boundary conditions (BC) and initial conditions (IC), etc., except from the turbulence models that will be tested herein) is described in-depth in [24, 25]. The mountain-valley geometry studied in this work (shown in Figure 1) is also the same as used in our previous research [24]. A proper mesh validation for the k–ε turbulence model can be found in [24]. While our numerical results were not validated against empirical field measurements, they were validated against large-eddy simulation (LES) results by Axelsen and van Dop [2, 26], who had validated their LES results against experimental measurements. Note that it is very difficult to find research in the literature reporting wind speed measurements in mountain-valley systems with configurations coincident with the simple geometry that we are using for our simulations, and data from non-similar geometries cannot obviously be used for validation purposes.

The most suitable settings for simulating thermally-driven flows identified in [24] are: 1) slip wall BC on the domain top surface; 2) uniform field temperature and pressure as IC; 3) fluid domain height of 2600 m; and 4) valley width W = 458 m (W does not affect significantly the thermally-driven wind convective cell, if W > 458 m [24]). Finally, the roughness length value used in this work is z_0 = 0.03 m, as in [27], and the slope angle is $\alpha = 20°$.

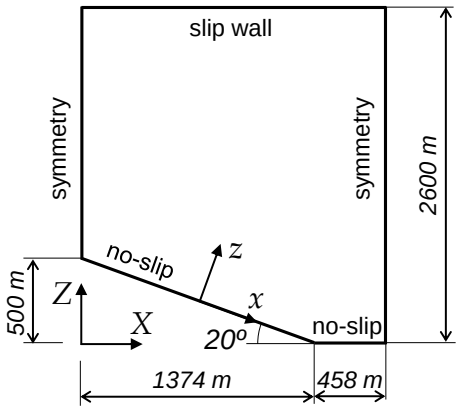

Figure 1. Studied mountain-valley geometry

2.1. Model - governing equations

If the flow field is assumed as a continuum, the mass, momentum, and energy conservation eqs. (Navier-Stokes eqs.) can be used to describe

the flow behaviour. Slope winds are due to natural convection, and the ABL formation is driven by temperature gradients. Thus, the energy and momentum conservation eqs. are coupled and, unless information from the energy equation goes into the momentum equation, the ABL growth cannot be solved. This can be overcome by using the Boussinesq approach. Here, if heat transfer is non-negligible, then the flow properties usually depend on temperature, and, if changes in density ρ are not significant, ρ can be considered constant in the unsteady and convection terms, while it is not so in the body force term of the Navier-Stokes eqs.

In this work, the Boussinesq approach is used [28, 29] with the following assumptions: the air is a Newtonian, dry, perfect gas at rest [27], ; radiation effects are negligible, as well as Coriolis effects, since the focus is on relatively small scales and local mechanisms in the near-ground-surface region [27, 28, 30]; the geostrophic wind velocity is zero; the diffusion is predominant in the direction normal to the slope, compared to along the slope; and the Brunt-Väisälä frequency N, a measure of the atmospheric stratification, is constant, as in [28, 29]. Applying the Boussinesq approach and the previous assumptions to the Navier-Stokes eqs.:

$$\nabla \cdot \vec{U} = 0 \tag{1}$$

$$\frac{\partial \vec{U}}{\partial t} + \nabla \cdot (\vec{U}\vec{U}) - \nabla \cdot (2\nu_{ef} D(\vec{U})) = = -\frac{1}{\rho_0}(\nabla p - \rho \vec{g}) \tag{2}$$

$$\frac{\partial T}{\partial t} + \nabla \cdot \left(\frac{\rho}{\rho_0}\vec{U}T\right) - \nabla \cdot \alpha_{eff} \nabla T = 0 \tag{3}$$

where $\vec{U}$ is the velocity vector, ν_{ef} the effective kinematic viscosity (sum of molecular kinematic viscosity ν and turbulent kinematic viscosity ν_t), $D(\vec{U}) = \frac{1}{2}\left(\nabla\vec{U} + (\nabla\vec{U})^T\right)$ the strain rate tensor, p the static pressure, T the temperature, ρ_0 the reference density at the reference temperature T_0, and α_{ef} the effective thermal diffusivity. In turn, ρ (updated in the temperature governing equation using the Boussinesq approach) and α_{ef} can be computed as follows:

$$\rho = \rho_0(1 - \beta(T - T_0)) \tag{4}$$

$$\beta = -\frac{1}{\rho}\left(\frac{\partial \rho}{\partial T}\right) \tag{5}$$

$$\alpha_{ef} = \frac{\nu}{Pr} + \frac{\nu_t}{Pr_t} \tag{6}$$

where $\beta = 3.5 \times 10^{-3}$ K^{-1} is the volume expansion coefficient (treated as constant), $\nu = 1.455 \times 10^{-5}$ m^2/s, $T_0 = 288.15$ K, and the laminar and turbulent Prandtl numbers $Pr = 0.7$ and $Pr_t = 0.9$.

Among the OpenFOAM solvers for heat transfer analysis that seem applicable for our research, *buoyantBoussinesqPimpleFoam* was chosen, which uses Navier-Stokes eqs. with Boussinesq approach. The simulations were performed using an Euler implicit time scheme, with time step 0.1 s, limiting the maximum value of the Courant number to ≈0.5.

2.2. Boundary conditions

As seen in Figure 1, no-slip wall is imposed as BC on the slope and valley, symmetry BC on both sides of the computational domain, and slip wall BC on its top. More details can be found in [24, 25]. While our previous work studied the formation of thermally-driven flows by imposing steady altitude-dependent temperature on the slope [24], the current work aims at studying the generation of such winds under time-dependent temperature (but constant with altitude) applied on the slope. To reproduce the diurnal cycle, the periodic temperature profile $T(t) = 288.15 - 10\sin(2\pi t/T_E)$ [K], where $T_E = 86\,400$ s, is set on the slope.

2.3. Turbulence models

The objective of this study is to simulate the diurnal cycle of thermally-driven winds using RANS eqs., which are the application of the Reynolds decomposition, consisting of expressing the solution variables as they appear in the instantaneous Navier-Stokes eqs. as the sum of a mean and a fluctuating component. To that end, k–ε, RNG k–ε, and k–ω SST models are considered. To determine k and ε, formulas typically used for inlet BC are considered [31]:

$$k(z) = \frac{u^{*2}}{\sqrt{C_\mu}} \text{ and } \varepsilon(z) = \frac{u^{*3}}{\kappa(z + z_0)} \tag{7}$$

where the turbulence viscosity constant $C_\mu = 0.09$ [32], the Von Kármán constant $\kappa = 0.41$, and the friction velocity u^* is given by:

$$u^* = \kappa \frac{U_{ref}}{ln\left(\frac{H_{ref}+z_0}{z_0}\right)} \tag{8}$$

Given that our BC do not include any inlet, the values of these parameters are only imposed as IC of the simulation and in the slope and valley wall functions. Thus, constant values are considered, taking as reference the value at $H_{ref} = 50$ m, where a reference velocity $U_{ref} \approx 1$ m s^{-1} is expected.

For k–ω SST, the turbulence specific dissipation rate is calculated as $\omega = \varepsilon/(C_\mu k)$. The obtained values of k, ε, and ω can be found in Table 1. Note that an analysis of the effect of these parameters is not included in this work, but this is of interest and will thus be considered in future research.

Table 1. Turbulence models and associated parameters (all RANS models use $k = 0.0102$ m^2 s^{-2})

Models	Parameters
RANS k–ε	$\varepsilon = 8.24 \times 10^{-6}$ m^2 s^{-3}
RANS RNG k–ε	$\varepsilon = 8.24 \times 10^{-6}$ m^2 s^{-3}
RANS k–ω SST	$\omega = 0.009$ s^{-1}
LES	$C_k = 0.094$
	$C_e = 1.048$

A preliminary study of LES is also presented. LES distinguishes between the large eddies in the flow, which are mainly determined by the geometry of the problem under study, and the smaller eddies that tend to be more universal. A filter is applied so that scales smaller than the filter size are removed from the variables, and their effect on the resolved scales is modelled by means of a turbulence model. Here, the Smagorinsky closure scheme [22, 23] is used, where:

$$\nu_t = C_k \Delta k^{0.5} \tag{9}$$

where C_k is the Kolmogorov constant and k is given by the solution of a quadratic eq. In this work, OpenFOAM default model coefficients are used (see Table 1). This study is made on the same mesh as the RANS study. It only aims at validating the applicability of the LES model to this problem, since a refined mesh would need to be adapted for the LES case, and the time step should be carefully chosen to properly solve the LES scales of the flow.

All simulations were run on 16 cores (of 8 GB of DDR4-2666 ECC RAM each) of a Dual AMD EPYC™ 7001 Series Processors. Table 2 shows the computational time needed to run 24 h of simulation time (864 000 time steps). Contrary to what is usual, LES shows shorter simulation time than the RANS models. The reason is that this is a preliminary study made on the same computational mesh as that for the RANS models. A finer mesh would be needed for LES, and possibly a smaller time step, which would lead to much higher computational time.

Table 2. Computational time (in days) to obtain 24 h of simulation time

Models	Time [days]
RANS k–ε	17.98
RANS RNG k–ε	13.30
RANS k–ω SST	18.63
LES	4.85

Between RANS models, RNG k–ε is the fastest one, k–ε and k–ω SST being ≈35% computationally more expensive. Note that for RANS models, at constant Δt, for 1000 s of simulation, computational time goes from ≈1 h in the katabatic phase (low velocity in the whole domain), to ≈15 h in the anabatic phase where, as seen in Section 3, flow velocity is higher and vortices appear. Future studies will include the possibility of considering adaptive time step.

3. RESULTS

Results were obtained for 2 diurnal cycles in all cases. Figure 2 shows the diurnal cycle of the maximum along-slope velocity measured at mid-slope for the different turbulence models. Though the time-dependent temperature profile shows symmetric range values (from −10 K at 6 h to +10 K at 18 h, with respect to the field initial temperature), it can be seen that the maximum speeds for katabatic flow (at 6 h) are much lower than for anabatic flow (at 18 h), as reported also in [33, 34, 35]. The diurnal timing of the speed peaks is consistent with the typical profiles of mountain breezes [36]. Finally, the values obtained for maximum velocity at mid-slope are very similar for all RANS models, though RNG k–ε shows more oscillations (especially in the anabatic phase), and the amplitude of the values obtained with LES is wider and with highly oscillating component in the anabatic phase.

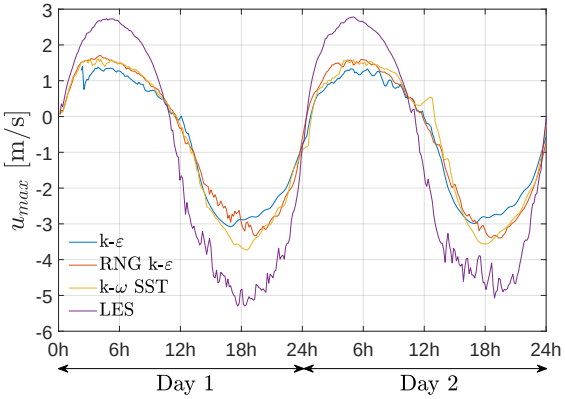

Figure 2. Diurnal cycle of maximum along-slope velocity u_{max} (at mid-slope) for the tested turbulence models

Figures 3 and 4 show velocity magnitude U corresponding to katabatic and anabatic configurations, respectively. In the katabatic case (Fig. 3), downslope velocity is observed, with very similar paterns for k–ε and RNG k–ε models. Contours obtained with k–ω SST model show higher vorticity in the top part of the domain, and LES ones lots of small vortices. While convective cells can hardly be perceived in the katabatic case, convective cells are clearly visible in the anabatic one (Fig. 4). In this case, as already seen in Fig. 2, the obtained velocities are significantly higher, and the choice of turbulence model does have some influence on the convective cell/vortex obtained: the cells from the k–ε and k–ω SST models are very similar, while the cell from the RNG k–ε model is a bit different, and LES shows lots of secondary cells, suggesting the need for a deeper study of the mesh and time step effects, to validate the choice of this turbulence model. Also note that though velocity contours seem to indicate that the domain height is affecting the results obtained from the anabatic simulations, a complete domain-height independence study [24], made in steady conditions, validated the choice of this height. It was further confirmed by performing a 24h-cycle simulation, with the k–ε model, using a height of 3250 m. In the area of interest, i.e. within 20 m above the slope ground, a maximum error of 1.5% was found when using H_D = 2600 m instead of 3250 m. It is also worth noting the increased difficulties in modelling the anabatic flow. This might be due to the fact that

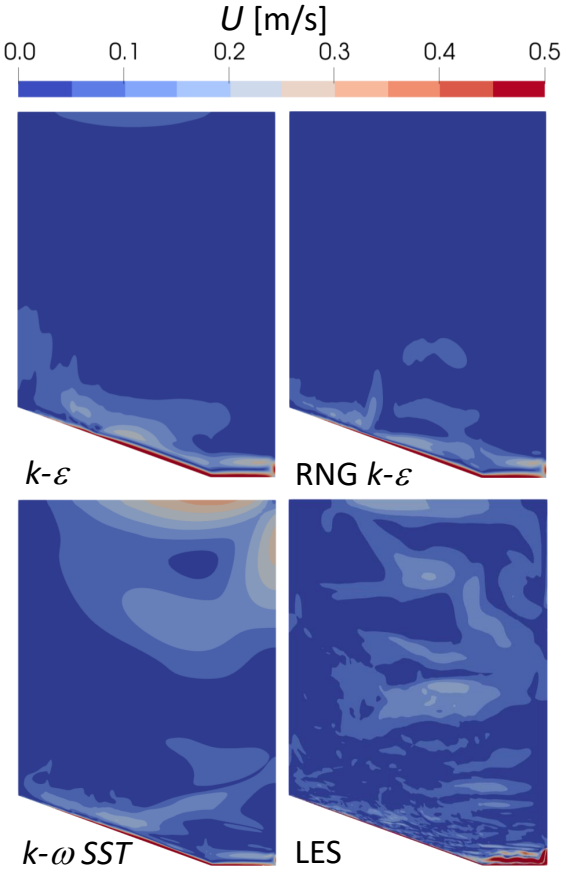

Figure 3. Katabatic flow (6 h, day2): velocity U for the tested turbulence models

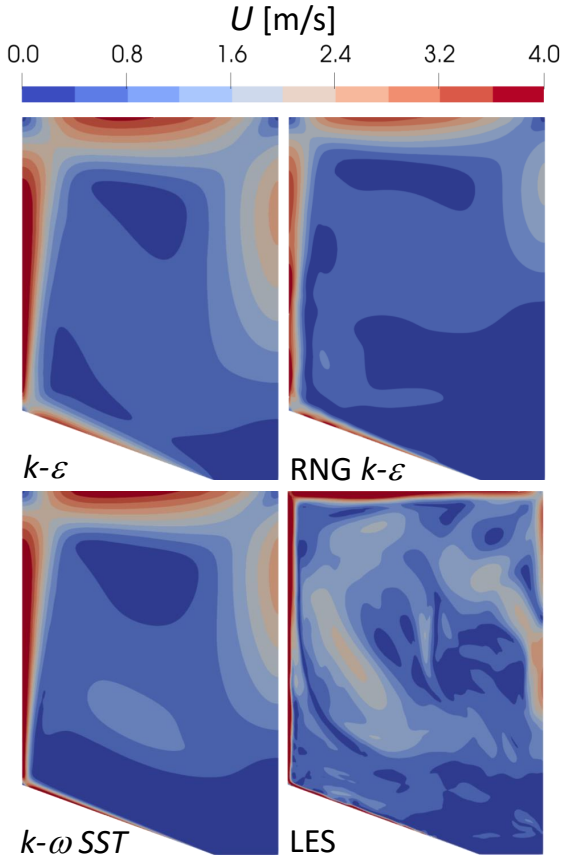

Figure 4. Anabatic flow (18 h, day2): velocity U for the tested turbulence models

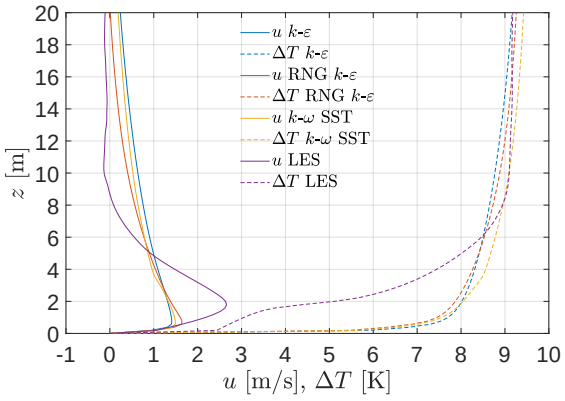

Figure 5. Katabatic flow: along-slope velocity u and ΔT profiles at 6 h (day2) for the tested turbulence models

anabatic flows are associated with absolute static instability inducing convective motions above a heated surface, as has been widely observed in the literature [28].

Figures 5 and 6 show the along-slope velocity and temperature profiles as a function of the slope-normal distance (z), at mid-slope, for the katabatic and anabatic cases (6 h and 18 h, day2), respectively.

Along-slope velocity profiles are expected to exhibit logarithmic behaviour, as for an ideal ABL [7]. In both cases, the flow velocity peak obtained with LES is clearly of higher magnitude and is observed at higher z than the peaks obtained with the RANS models. It can also be observed that the results obtained with RANS models both for velocity and temperature are very similar in the katabatic case, while in the anabatic case they show more discrepancies, especially in the results obtained with k–ω SST, which show a smoother temperature profile close to the ground, leading to a higher value of the along-slope flow velocity. As for the k–ε anabatic results, the temperature profile is the one showing a faster decrease in the near-ground area, but then, above ≈15 m, temperature decreases slower than with any other RANS method. This leads to the lowest absolute peak value of velocity (below 3 m/s vs above 3.5m/s for the other methods), but then the absolute velocity value decreases slower than with the other RANS methods.

Figure 7 shows the along-slope velocity u at mid-slope, at different slope-normal distances, for the four tested turbulence models. This representation can be useful when thinking of wind energy applications, in order to get an estimation of the magnitude of the thermally-driven wind speed for different heights. For instance, all results show that,

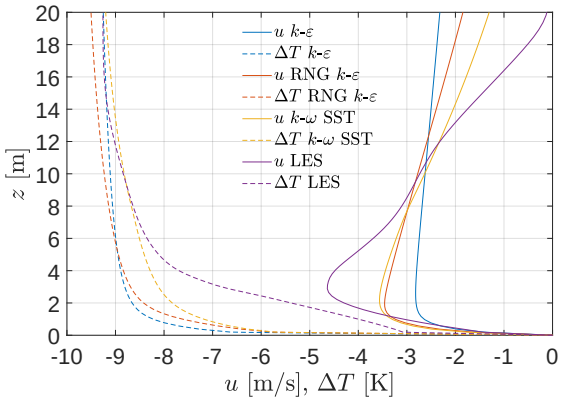

Figure 6. Anabatic flow: along-slope velocity u and ΔT profiles at 18 h (day2) for the tested turbulence models

for z between 5 and 10 m, katabatic velocities remain extremely low (≈1 m/s). Wind energy generation could only be envisaged in the current configuration (no synoptic wind considered, slope angle of 20°, diurnal temperature difference between the slope and the air of 20 K, etc.) during the anabatic phase (velocities around 2 or 3 m/s) with small wind turbines. As for the differences observed in the results obtained with the four tested turbulence models, again, LES (Fig. 7d) and (to a less extent) RNG k–ε (Fig. 7b) results show more oscillations in the velocity profile, while k–ε (Fig. 7a) and k–ω SST (Fig. 7c) show similar, smoother profiles. Again, k–ω SST leads to higher (in absolute terms) values of the along-slope flow velocity, especially at low slope-normal distance (z = 2.5 and z = 5 m). The decrease of velocity with z is very fast with LES (u remains close to 0 all the time for z > 20 m), and quite fast also with RNG k–ε and k–ω SST models. With the k–ε model, the shape of the velocity profile at 40 m is similar to the one at lower values of z, given that, as also observed in Fig. 6, the decrease of velocity with z is much slower.

4. CONCLUSIONS

This work reports a preliminary comparison of turbulent models used with OpenFOAM for studying the diurnal cycle of thermally-driven winds in mountain-valley systems. Our results suggest that k–ε and k–ω SST models are the most promising models, with a small advantage to k–ω SST for the near wall simulation, as it gives a smoother temperature transition away from the slope (especially in the anabatic phase), leading to more realistic vertical profiles of along-slope flow velocity. As for k–ε, it leads to a much slower decrease of velocity when going away from the ground. LES model was able to simulate this type of winds but complementary simulations using finer mesh are needed to confirm its suitability. In next steps, the results obtained for these idealised mountain-valley systems with RANS

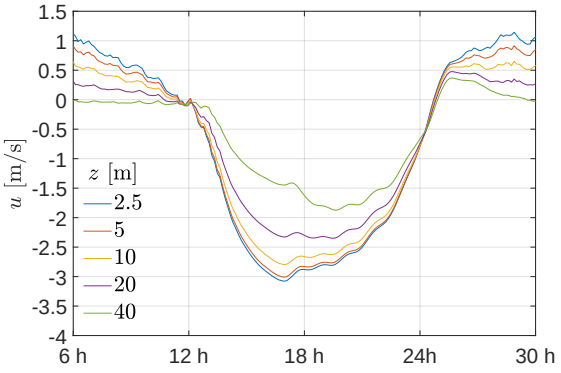

(a) k-ε

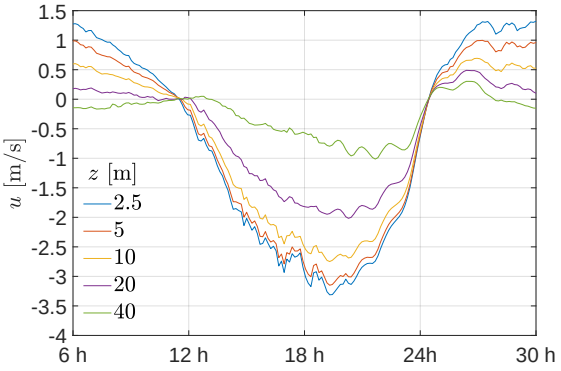

(b) RNG k-ε

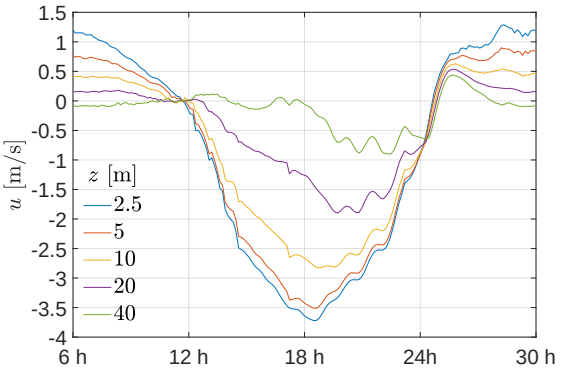

(c) k-ω SST

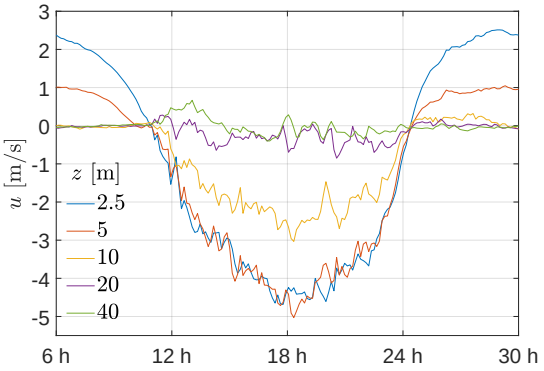

(d) LES

Figure 7. Along-slope velocity u at mid-slope, at different slope-normal distances, for the tested turbulence models

and LES models will be validated against direct numerical simulations (DNS), as well as against results from suitable experimental campaigns reported in the literature [37, 38, 36].

ACKNOWLEDGEMENTS

This work is supported by the project PID2019-105162RB-I00 funded by MCIN/AEI/10.13039/501100011033 and by the project 2017 SGR 1278 from the AGAUR *Generalitat de Catalunya*.

REFERENCES

[1] Balogh, M. G., Parente, A., and Benocci, C., 2012, "RANS simulation of ABL flow over complex terrains applying an enhanced k-epsilon model and wall function formulation: Implementation and comparison for Fluent and OpenFOAM", *J Wind Eng Ind Aerodyn*, Vol. 104–106, pp. 360–368.

[2] Axelsen, S. L., and van Dop, H., 2009, "Large-eddy simulation of katabatic winds. Part 2: Sensitivity study and comparison with analytical models", *Acta Geo*, Vol. 57, pp. 837–856.

[3] Alinot, C., and Masson, C., 2005, "k-epsilon model for the atmospheric boundary layer under various thermal stratifications", *J Sol Energy Eng ASME*, Vol. 127, pp. 438–443.

[4] An, K., Fung, J. C. H., and Yim, S. H. L., 2013, "Sensitivity of inflow boundary conditions on downstream wind and turbulence profiles through building obstacles using a CFD approach", *J Wind Eng Ind Aerodyn*, Vol. 115, pp. 137–149.

[5] Batt, R., Gant, S. E., Lacome, J.-M., and Truchot, B., 2016, "Modelling of stably-stratified atmospheric boundary layers with commercial CFD software for use in risk assessment", *Proc 15th Int Symp Loss Prev Saf Promot, Chem Eng Trans*, Freiburg, Germany, pp. 61–66.

[6] Franke, J., Sturm, M., and Kalmbach, C., 2012, "Validation of OpenFOAM 1.6.x with the German VDI guideline for obstacle resolving micro-scale models", *J Wind Eng Ind Aerodyn*, Vol. 104–106, pp. 350–359.

[7] Bautista, M. C., 2015, "Turbulence Modelling of the Atmospheric Boundary Layer over Complex Topography", Ph.D. thesis, Université de Québec, École de Technologie Supérieure.

[8] Hu, P., Li, Y., Cai, C. S., Liao, H., and Xu, G. J., 2013, "Numerical simulation of the neutral equilibrium atmospheric boundary layer using the SST k–ω turbulence model", *Wind Struct*, Vol. 17, pp. 87–105.

[9] Yang, Y., Xie, Z., and Gu, M., 2017, "Consistent inflow boundary conditions for modelling the neutral equilibrium atmospheric boundary layer for the SST k–ω model", *Wind Struct*, pp. 465–480.

[10] Hamisu, M. T., Jamil, M. M., Umar, U. S., and Sa'ad, A., 2019, "Numerical study of flow in asymmetric 2D plane diffusers with different inlet channel lengths", *CFD Lett*, Vol. 11, pp. 1–21.

[11] Michalcová, V., Lausová, L., Skotnicová, I., and Pospísil, S., 2017, "Computational simulations of the thermally stratified atmospheric boundary layer above hills", *Procedia Eng*, Vol. 190, pp. 134–139.

[12] Samala, B. P. R., 2016, "Active Flow Control of Boundary Layer Separation on Airfoils Using Fluidic Oscillators", Ph.D. thesis, Universitat Politècnica de Catalunya, Dept. of Physics.

[13] Bhuiyan, A. A., Karim, R. M., Hart, J. T., Rahman, M. M., and Naser, J., 2016, "Experimental and numerical investigation of coherent structure dynamics on mass transfer in a separated cavity flow", *Exp Therm Fluid Sci*, Vol. 76, pp. 146–162.

[14] Flores, F., Garreaud, R., and Muñoz, R. C., 2014, "OpenFOAM applied to the CFD simulation of turbulent buoyant atmospheric flows and pollutant dispersion inside large open pit mines under intense insolation", *Comput Fluids*, Vol. 90, pp. 72–87.

[15] Flores, F., Garreaud, R., and Muñoz, R. C., 2013, "CFD simulations of turbulent buoyant atmospheric flows over complex geometry: solver development in OpenFOAM", *Comput Fluids*, Vol. 82, pp. 1–13.

[16] Pereira, F. S., Grinstein, F. F., Israel, D. M., Rauenzahn, R., and Girimaji, S. S., 2021, "Modeling and simulation of transitional Taylor-Green vortex flow with partially averaged Navier-Stokes equations", *Phys Rev Fluids*, Vol. 6, p. 054611.

[17] Garcia, M., and Boulanger, P., 2006, "Low altitude wind simulation over Mount Saint Helens using NASA SRTM digital terrain model", *Proc 3rd Int Symp 3D Data Proces, Visualiz, Trans*, Univ North Carolina, Chapel Hill, USA.

[18] Hussein, A. S., and El-Shishiny, H., 2009, "Influences of wind flow over heritage sites: a case study of the wind environment over the Giza Plateau in Egypt", *Environ Modell Software*, Vol. 24, pp. 389–410.

[19] Garcia, M., and al., 2008, "CFD analysis of the effect on buoyancy due to terrain temperature based on an integrated DEM and Landsat infrared imagery", *Ing Cienc*, Vol. 4, pp. 65–84.

[20] Pedruelo, X., 2009, "Modelling of wind flow over complex terrain using OpenFOAM", Ph.D. thesis, Dept Technol Built Environ, University of Gavle.

[21] Churchfield, M., 2010, "A description of the OpenFOAM solver buoyantboussinesqpisofoam", *Tech. rep.*, National Renewable Energy Laboratory, National Wind Technology Center.

[22] Majander, P., and Siikonen, T., 2002, "Evaluation of Smagorinsky-based subgrid-scale models in a finite-volume computation", *Int J Numer Methods Fluids*, Vol. 40, pp. 735–744.

[23] Cao, S., Wang, T., Ge, Y., and Tamura, Y., 2012, "Numerical study on turbulent boundary layers over two-dimensional hills - Effects of surface roughness and slope", *J Wind Eng Ind Aerodyn*, Vol. 104, pp. 342–349.

[24] Athota, R. B., Rojas, J. I., Arias, S., and Montlaur, A., 2022, "Simulations of thermal wind formation in idealised mountain-valley systems using OpenFOAM", Available at SSRN: `https://ssrn.com/abstract=4086430` or `https://dx.doi.org/10.2139/ssrn.4086430`.

[25] Athota, R. B., Rojas, J. I., and Montlaur, A., 2021, "OpenFOAM computational fluid dynamics simulations of thermal wind generation in mountain/valley configurations", *14*$^{\text{eff}}$ *WCCM & ECCOMAS Congress*.

[26] Axelsen, S. L., and van Dop, H., 2009, "Large-eddy simulation of katabatic winds. Part 1: Comparison with observations", *Acta Geophys*, Vol. 57, pp. 803–836.

[27] Brun, C., Blein, S., and Chollet, J., 2017, "Large-eddy simulation of a katabatic jet along a convexly curved slope. Part I: Statistical results", *J Atmos Sci*, Vol. 74, pp. 4047–4073.

[28] Fedorovich, E., and Shapiro, A., 2009, "Structure of numerically simulated katabatic and anabatic flows along steep slopes", *Acta Geo*, Vol. 57, pp. 981–1010.

[29] Shapiro, A., Burkholder, B., and Fedorovich, E., 2012, "Analytical and numerical investigation of two-dimensional katabatic flow resulting from local surface cooling", *Boundary-Layer Meteorol*, Vol. 145, pp. 249–272.

[30] Giometto, M. G., Katul, G. G., Fang, J., and Parlange, M. B., 2017, "Direct numerical simulation of turbulent slope flows up to Grashof number $Gr = 2.1 \times 10^{11}$", *J Fluid Mech*, Vol. 829, pp. 589–620.

[31] Richards, P., and Hoxey, R., 1993, "Appropriate boundary conditions for computational wind engineering models using the k—e turbulence model", *J Wind Eng Ind Aerodyn*, Vol. 47, p. 145–153.

[32] Richards, P. J., and Norris, S. E., 2011, "Appropriate boundary conditions for computational wind engineering models revisited", *J Wind Eng Ind Aerodyn*, Vol. 99, pp. 257–266.

[33] Svensson, G., Holtslag, A. A. M., Kumar, V., Mauritsen, T., Steeneveld, G. J., Angevine, W. M., Bazile, E., Beljaars, A., de Bruijn, E. I. F., Cheng, A., Conangla, L., Cuxart, J., Ek, M., Falk, M. J., Freedman, F., Kitagawa, H., Larson, V. E., Lock, A., Mailhot, J., Masson, V., Park, S., Pleim, J., Söderberg, S., Weng, W., and Zampieri, M., 2011, "Evaluation of the diurnal cycle in the atmospheric boundary layer over land as represented by a variety of single-column models: The second GABLS experiment", *Boundary-Layer Meteorol*, Vol. 140, pp. 177–206.

[34] Giovannini, L., Laiti, L. Serafin, S., and Zardi, D., 2017, "he thermally driven diurnal wind system of the Adige Valley in the Italian Alps", *Q J R Meteorol Soc*, Vol. 143, pp. 2389–2402.

[35] Barcons, J., Avila, M., and Folch, A., 2019, "Diurnal cycle RANS simulations applied to wind resource assessment", *Wind Energy*, Vol. 22, pp. 269–282.

[36] Román-Gascón, C., Yagüe, C., Arrillaga, J. A., Lothon, M., Pardyjak, E. R., Lohou, F., Inclán, R. M., Sastre, M., Maqueda, G., Derrien, S., Meyerfeld, Y., Hang, C., Campargue-Rodríguez, P., and Turki, I., 2019, "Comparing mountain breezes and their impacts on CO_2 mixing ratios at three contrasting areas", *Atmos Res*, Vol. 221, pp. 111–126.

[37] Charrondière, C., Brun, C., Sicart, J., Cohard, J., Biron, R., and Blein, S., 2020, "Buoyancy effects in the turbulence kinetic energy budget and Reynolds stress budget for a katabatic jet over a steep Alpine slope", *Boundary-Layer Meteorol*, Vol. 177, pp. 97–122.

[38] Charrondière, C., Brun, C., Cohard, J., Sicart, J., Obligado, M., Biron, R., Coulaud, C., and Guyard, H., 2022, "Katabatic winds over steep slopes: Overview of a field experiment designed to investigate slope-normal velocity and near-surface turbulence", *Boundary-Layer Meteorol*, Vol. 182, pp. 29–54.